NASA CR-174,172

A Reproduced Copy

OF

NASA CR-174,172

NAG-1-483

THE ROLE OF FREESTREAM TURBULENCE SCALE IN SUBSONIC FLOW SEPARATION

J. Leith Potter
W. R. Seebaugh
R. Joel Barnett
Rajiv B. Gokhale

Sponsored Research Project RG-5997
NASA Research Grant NAG-1-483

Interim Progress Report No. 1

December 31, 1984

VANDERBILT UNIVERSITY
School of Engineering
Department of Mechanical & Materials Engineering
Nashville TN 37235

Interim Progress Report 1

THE ROLE OF FREESTREAM TURBULENCE SCALE IN SUBSONIC FLOW SEPARATION

J. Leith Potter, Co-Principal Investigator
W. R. Seebaugh, Co-Principal Investigator
R. Joel Barnett, Graduate Student
Rajiv B. Gokhale, Graduate Student

Department of Mechanical and Materials Engineering
School of Engineering
Vanderbilt University
Nashville, TN 37235

Sponsored Research Project RG-5997
NASA Research Grant NAG-1-483

Period Covered: 1 July 1984 - 31 December 1984

Contents

List of Figures

List of Tables

INTRODUCTION

This is a report of progress during the period from 1 July to 31 December, 1984. As such, it concerns the start-up phase of the research. The current grant extends from 1 July 1984 to 30 June 1985.

The objective of this work is the clarification of the role of freestream turbulence scale in determining the location of boundary layer separation. An airfoil in subsonic wind tunnel flow is the specific case studied. Hot-film and hot-wire anemometry, liquid-film flow visualization and pressure measurements are the principal diagnostic techniques in use. The Vanderbilt University subsonic wind tunnel (Fig. 1) is the flow facility being used.

Inasmuch as this is the initial progress report, it is devoted to the preparatory phase of the planned effort. However, it is shown that solid progress has been made, and the project goals should be met despite several unanticipated technical problems which are described later. The first year of the proposed two-year effort is largely devoted to experimentation, and that is reflected in the discussion to follow.

DESCRIPTION OF EQUIPMENT AND METHODS

Wind Tunnel

The Vanderbilt University Enginering School Wind Tunnel is shown in Figures 1-3. A top view of the tunnel is not shown because the structure is of square cross section upstream of the diffuser, and the latter component varies from square to circular as it extends downstream. Except for the fan section, the tunnel shell is made of fiberglass, giving a very smooth interior surface. A summary of flow conditions is presented in Table 1.

TABLE 1. VUES Wind Tunnel Flow Data

Assumed room air at typical conditions of 1.002×10^5 N/m^2 (29.60 in.Hg) and 295 K (72°F). No model installed in tunnel.

Test Section	Max. Speed	(Re/L) x 10^{-4}
1.02 x 1.02 m (40 x 40 in.)	11.2 m/s 36.7 fps	71.3 m^{-1} 1.81 in.$^{-1}$
0.411 x 0.411 m (16.2 x 16.2 in.)	74.7 m/s 245 fps	462 m^{-1} 11.7 in.$^{-1}$

The smaller, higher speed, 0.4-m section is the normal test section, and all subsequent comments will pertain to that area unless specific reference is made to the 1-m section.

A shroud, honeycomb, and two screens are installed at the wind tunnel entrance. Figure 4 is a view looking into the entrance area. Prior to that modification, the flow into the upstream end of the tunnel was not sufficiently uniform nor steady. The combination of the size of the room housing the tunnel, the relatively high air speeds, and the relatively short distance from exit to entrance of the tunnel created this problem, which is not unusual with the open-return type of wind tunnel. Addition of these components to the entrance dramatically improved the uniformity and steadiness of the flow with only a minor penalty in top speed. In addition to the hot-wire measurements of turbulence intensity reported later, extensive studies of the flow were made with the aid of tufts of yarn taped to the interior of the tunnel, static pressure measurements, and pitot-static probing.

The honeycomb is comprised of plastic impregnated paper having a thickness of 0.2 mm. There are two layers making up the honeycomb.

In each layer the cells, or openings, are approximately triangular in crossection, with a base of 9.5 mm and height of 8 mm. Streamwise dimension of the assembly is 64 mm, giving a length-to-hydraulic diameter ratio of approximately 7.

Two fiberglass screens with 6.3 mesh/cm (16/in.) were installed to reduce turbulence. Additional screens may be inserted if it is later desired to study boundary layer transition or other phenomena requiring very low freestream turbulence. Maximum freestream velocity would be reduced, of course. Relative turbulence intensity in the test section at speeds below roughly 60 m/s is 0.27 to 0.29 percent with the present set of screens.

Velocity distribution laterally across the 0.4-m test section, measured by hot-wire and pitot-static probes, is constant to within ± 1 percent in the central 0.3 m (12 in.) at a mean velocity of 60 m/s (200 fps). Longitudinal velocity gradient in the test section is virtually zero at all of the usual test conditions.

In addition to the quantitative data given above, pressure measurements have been made along the diffuser and contraction sections to ascertain that flow separation does not occur there, and the lack of correlation between hot-film probe signals at wide lateral spacing in the test section indicates that there is no pressure fluctuation such as could arise from the wind tunnel fan or a large-scale flow disturbance. Examination of both hot-wire and pressure data using a frequency analyzer has revealed no dominant frequencies in the range of detection by that instrument other than a 60-Hz noise that appeared in the analyzer even when no tunnel probes were connected. Small areas of separation were discovered in the four corners at the beginning of the wind tunnel contraction which follows downstream of the 1-m cross section.

A future improvement could be effected by fairing these regions so as to make the transition less abrupt.

A flexible coupling at the downstream end of the diffuser reduces vibration that would be caused by the centrifugal fan and motor. The laboratory floor is of thick concrete and quite rigid. However, at higher speeds there is a small amount of vibration in the tunnel shell, so sensitive probes are mounted onto the laboratory floor.

Pressure and Hot-Wire/Hot-Film Systems

In addition to an array of older dial gauges and liquid-column manometers, the Vanderbilt Wind Tunnel is equipped with a Scanivalve Corporation DSS 24C MK3 electronic switching-valve pressure transducer system. When this is used in conjunction with a manually-operated Norgren Fluidics 10-port switch, up to 34 pressure measurement channels are available. Because the Scanivalve pressure transducer range is too high for accurate results in the present program, a MKS Baratron Model 170M-6C precision pressure transducer with a full-scale range of 100 mm Hg is being used.

Three channels of hot-wire instrumentation are available. These include one Thermo Systems, Inc. (TSI) Model 1050 and two TSI Model 1010 anemometer systems. Each anemometer channel has a linearizer, a TSI Model 1052A being used with the 1050 anemometer and TSI Model 1072 linearizers with the 1010 anemometers. A TSI 1015C Correlator is used for correlation of signals from the anemometers. The primary voltage measurements, D.C., rms, and mean square, are obtained with a TSI Model 1076 digital voltmeter. This instrument may be operated with time constants of 0.1, 1.0, 10 and 100 seconds.

Data acquisition currently is accomplished with an Interactive

Structures, Inc., Model AI13 analog-to-digital converter coupled to an Apple IIe computer. Work on software in progress is expected to extend the scope of the correlation data and expedite the data taking process.

The hot-wire/hot-film probes are standard TSI models. The hot-wire sensors are platinum coated tungsten on gold plated needle-type supports. Diameter of sensing element is 3.8 μ (0.00015 in.) and the length is 1.27 mm (0.050 in.). Corresponding dimensions of the hot film probes are 51 μ (0.002 in.) and 1.0 mm (0.040 in.). The sensor films are platinum with an alumina coating. Fused quartz substrates and gold plated needle-type supports are used.

Detection of Separation By Liquid Films

Although location of boundary layer separation can be found with the hot-wire or small impact-pressure probes, it is obviously advantageous to have a method that gives a larger-scale, visual result. Liquid films of various solutions were painted onto an airfoil and tested in the tunnel. It was found that a mixture of the following approximate proportions (by volume) served our purpose:

50 percent water
35 percent dry powdered poster paint
10 percent glycerine
~ 5 percent Kodak Photo Flo.

This solution was brushed onto an airfoil surface that had been wetted with a film of soapy water.

Figure 5 shows the resulting indication of the region of separation on the airfoil which was at an angle of attack sufficient to provoke separation near the midchord. No liquid was applied ahead of 10-percent chord. It may be noted that rather extensive reversal of flow at the trailing edge in this case cleaned the liquid film off of the airfoil over the downstream

15 percent of the chord. The film, pushed from both upstream and downstream directions, collected between 60 and 85 percent of the chord. The paint film at the downstream edge of the separated area was wet enough at the termination of air flow that some ran into the otherwise clean trailing edge region as seen in the photograph. The upstream separation at 60 percent chord is very well defined, and it appears that this technique will be satisfactory for the remaining research.

PRELIMINARY EXPERIMENTS

Turbulence Intensity

The relative turbulence intensity is defined as

$$T_q' = (\overline{q^2})^{1/2}/Q, \qquad (1)$$

where $\overline{q^2}$ = the mean square of the fluctuating component of the mean velocity, Q.

With reference to the following sketch of orthogonal axes and velocity components, let

U_∞ = mean or freestream velocity

$V_\infty = W_\infty = 0$ = mean velocity along y or z, respectively

u,v,w = fluctuating velocities in x,y,z, directions, respectively.

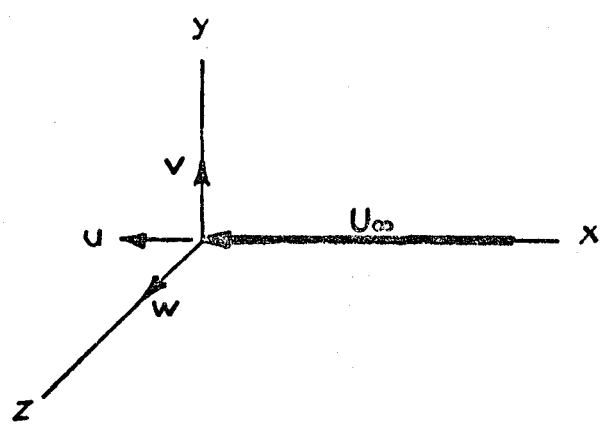

Then a hot-wire which is perpendicular to the x axis and parallel to the z axis will be affected almost exclusively by $(U_\infty + u)$ and v. If u/U_∞ and v/U_∞ are small, Bradshaw (Ref. 1) has shown that the fluctuating part of the effective velocity acting on the wire is

$$u + 0.5[(v^2 - \overline{v^2})/U_\infty].$$

Bradshaw also states that the ratio of measured $\overline{u^2}$ to true $\overline{u^2}$ is of the order of

$$1 + \left(\frac{\overline{v^2}}{U_\infty \sqrt{\overline{u^2}}}\right)S + 0.5\left(\frac{\overline{v^2}}{U_\infty \sqrt{\overline{u^2}}}\right)^2 + \text{---}$$

where $S = \overline{u^3}/(\overline{u^2})^{3/2} \approx -2$ outside a boundary layer.

If $\overline{v^2} \approx \overline{u^2}$ is assumed, and the higher level of $\sqrt{\overline{u^2}}/U_\infty \approx 0.01$ for the present experiments is also assumed, the ratio of measured and true $\overline{u^2}$ is approximately 0.98. When there is no model present to create asymmetry in the flow, in our tunnel, having a square cross-section upstream of the diffuser, we expect $\overline{v^2} \doteq \overline{w^2}$ at points not too close to the walls. Therefore, in what follows, the freestream relative turbulence intensity is taken to be

$$T' = \sqrt{\overline{u^2}}/U_\infty = u'/U_\infty, \qquad (2)$$

where u' is measured by a hot-wire normal to U_∞.

It will be recalled that earlier researchers in the field of turbulence measured sphere drag or a representative pressure coefficient as a function of Reynolds number and designated a Reynolds number, Re_c, corresponding to particular values of the drag coefficient or pressure coefficient as an indirect measure of turbulence of the flow. Dryden, et al., in Ref. 2

gave a correlation of T' and Re_{C_p} based on the sphere test, and the correlation was extended in Ref. 3. As an independent and simpler experiment which would furnish data to compare with the hot-wire measurements, a sphere test was performed.

Figure 6 gives the dimensions of the sphere and mounting sting used for the present experiment. The measured data are presented in Figure 7. We define

$$C_p = (p_o' - p_b)/q_\infty \tag{3}$$

where

p_o' = stagnation pressure,

p_b = pressure on the sphere 157.5 deg from the stagnation point,

q_∞ = freestream dynamic pressure

and $$Re = U_\infty d/\upsilon_\infty, \tag{4}$$

where

U_∞ = freestream velocity, υ_∞ = kinematic viscosity

d = sphere diameter.

The critical Reynolds number corresponds to $C_p = 1.22$.

It must be recognized that if T' varies with U_∞ and all data are taken with one sphere diameter, then the curve in Figure 7 represents a composite which is not exactly like a curve for constant U_∞. This difference normally would be seen in the transition region. Under these circumstances, tests at discrete values of U_∞, using a number of spheres of varying diameters, would produce a set of curves. However, T' usually varies only slightly with U_∞ in a given wind tunnel and the simplification of one sphere and varying velocity was adopted.

Referring to Figure 7, it is noted that Re_c for the Vanderbilt wind

tunnel is 335,000. When that is compared with the correlated data in Figure 8, a T' in remarkably good agreement with our hot-wire data (approximately 0.28 percent) is indicated. The small scale of the figure in Ref. 2 prevents an exact reading. Considering that the sphere surface was not entirely smooth and there was visible vibration in the sphere support system, the value of Re_c possibly would be increased by more careful testing. At any rate, the agreement is most encouraging and seems to support the hot-wire data.

Hot-Film Compared with Hot-Wire Data

The plan was to generally use hot-film probes because of their greater strength compared to hot wires. Because the hot wires are known to exhibit greater sensitivity and better accuracy than the hot films, it was intended that the hot wire be used for absolute measurement of T' and as a comparative standard for the hot-film probes.

In accord with that plan, T' as a function of tunnel freestream velocity, U_∞ was measured, and the result is shown in Figure 9. The floor-mount and side-mount designations refer to two different supporting structures for the same probe. Both are ultimately supported from the concrete floor of the room, but the so-called floor mount is somewhat more rigid. That extra stability apparently did not make a significant difference in the results. The upward trend of T' at higher speeds is quite repeatable and may be caused by the increased flow rate through the room as the open-circuit wind tunnel speed control is advanced. As is demonstrated hereafter, the hot-film probes all displayed a much more pronounced climb in T' values above roughly 45 m/s. There may be more than one reason for this, but the most plausible hypothesis is that vortex shedding from the probe is mainly responsible for the apparently excessive turbulence readings.

It is noted that the Reynolds number, based on cylindrical hot-film sensor

diameter of 0.05 mm (0.002 in.) is approximately 140-180 where the apparently false increase in turbulence intensity begins. This is also where vortex shedding frequency is known to be increasing markedly. (See, e.g, Ref. 4 pages 30-31.)

Figure 10 gives typical data on T' obtained with hot-film probes in several configurations. At this point further explanation of terms is necessary. The hot-wire probes always are mounted so that the needles supporting the wire sensor are essentially parallel with flow direction. However, the hot-film probes are classified as "fork" mounted or "L" mounted. In the former case, the needles supporting the sensor element are perpendicular to the flow; in the latter case, goose-neck or L-shaped adapters are used so that the needles are parallel to the flow. The results vary between fork, goose-neck and L mounts. There is also variation above the 45 m/s level between hot-flm probes on the same mounting system. It was our ill fortune to choose 60 m/s as a tunnel speed and hot-film probes for carrying out preliminary comparisons of T' measurements, and a great amount of frustration ensued because of the poor repeatability. It was also apparent that the T' data all were much too high to be compatible with the T' inferred from the sphere critical Reynolds number found earlier. Only after testing across the tunnel speed range and obtaining T' by using a hot-wire probe was our puzzle resolved. We are unaware of any reports of this failing of hot-film probes in earlier publications. If the problem arose only when fork mounted, it would be implied that vortex shedding from the needles in crossflow is responsible. However, the same failing in only lesser degree appears when L-mounted probes are used. Vibration of the needles was suspected, but the application of candle wax in the form of a fillet to stiffen the needles only partially alleviated the problem as shown in Figure 10. Coupling a

frequency analyzer to the probe signal did not reveal any dominant frequency in the 0-20 kHz range of the analyzer. It appears that the rapidly increasing, very high frequency vortex shedding from the sensor element itself is the probable cause of the spurious readings at higher speeds. The hot films will be used only for comparative or differential measurements and only at speeds below 45 m/s in our case. We will continue to use the term hot-wire in a generic sense to include both types of probe, but the type will be specified when specific measurements are discussed.

Turbulence Scales

To describe turbulent motion quantitatively, in addition to relative intensity, the concept of turbulence scales has been formulated, (cf. Refs. 5-7). Scales in time and in space, as well as scales in longitudinal and transverse directions, are considered.

Defining the scales of turbulence usually involves correlations between velocity components at a fixed point in a flow or between components separated in either time or space. In either case, the correlation will be a function of time lapse or distance between the points. Distinctions are made between small fluid elements (fluid "particles") and larger elements (fluid "lumps"). The former are comparable to the micro scales, the latter comparable to the integral scales. Eulerian and Langrangian descriptions are useful. In the first, the variation of a property with respect to a fixed coordinate system is considered; in the latter, the variation of the property connected with a given fluid particle or fluid lump is determined.

Traditionally, the integral scale usually has been used in efforts to determine the role of turbulence scale in connection with drag, heat transfer, separation, transition, etc. However, other scales in the spectrum of turbulence have been identified, and several recent reports of studies of

the influence of freestream turbulence on boundary layers present discussions based exclusively on a dissipation length scale (Ref. 8-9). The latter is attractive in that it is generally easier to measure.

With regard to the scale of most influence on boundary layer separation, the issue would appear to be whether gradient-type transport of turbulence properties, related to the micro- or dissipation lengths, or transport by bulk movement related to the integral scales is the dominant process. One is attracted to the idea that bulk movement, and therefore intergral scale, is the most likely candidate. The almost universal choice of early investigators of scale effect on boundary layers has been the integral scales (e.g., Ref. 2). Numerous other examples of this choice could be cited. However, in 1974, Bradshaw (Ref. 10) proposed that a dissipation scale be used for interpretation of the effects of turbulence scale upon boundary layers, and this is the path followed by most of the recent investigators. One may say that the longitudinal dissipation length scale is the "modern" parameter. We are in the process of deciding how the bulk of our data will be presented. Because both scales will be measured and discussed later, each is defined here.

Integral Scale: References (5-7), for example, contain detailed discussions of this topic, so we only define the particular approach followed in the present work. Referring to the sketch following Eq. (1), consider how the size of turbulent eddies will be reflected by correlations of velocity fluctuations at different points in space or time. If two points in space have coordinates (o,o,z) and (o,o,z+r), the covariance of the u component of fluctuating velocity is $\overline{u(z) \cdot u(z+r)}$, and a correlation coefficient is defined as

$$R_{uz} = \overline{u(z) \cdot u(z+r)} / [\overline{u^2}(z) \cdot \overline{u^2}(z+r)]^{1/2} \qquad (5)$$

The correlation with separation r is indicative of the strength of eddies with dimensions exceeding r in the given direction, z. A length defined as

$$\ell_{uz} = \int_0^\infty R_{uz} dz \tag{6}$$

represents the typical z dimension of the energy-containing eddies in the flow. This is one of the integral scales mentioned earlier. Considerations of other coordinate directions and velocity components leads to the other integral scales. An example of a preliminary measurement follows.

Delays in acquiring some new equipment made it expedient to begin by measuring the integral scale in the cross-flow or lateral direction, z, as defined in the sketch following Eq. (1). This was done by use of two hot-film probes, one fixed in position and the other moved by increments along the z axis by the mechanical traversing system shown in Figure 11. Signals from the two probes were fed to the TSI anemometer systems already described, and the spatial correlation, R_{uz}, was obtained with the aid of the Apple computer which sampled a large number of signals and provided an average for each increment in z.

To initiate the present experiments with grid-produced turbulence, the grid having the largest planned mesh size was constructed. It will be identified as the 10-cm grid hereafter. The dimensions are given in Figure 12, and Figure 13 contains photographs of the installation in the tunnel's 1-m section. Mounting is by means of four tracks running the length of the 1-m test section, so a range of longitudinal positions of the grids is available.

Because of the location of the grids upstream of a contraction, a direct comparison of characteristics of the grid-generated turbulence with most other published data is not valid. A contraction is known to produce

significant changes in the turbulence and it is made clear in Ref. 11 that these effects vary with not only the geometry of the contraction, but also the characteristics of the turbulence in the fluid entering the contraction section. At this time there does not seem to be any other data which pertain to our specific set of conditions. One may only comment that the lateral scale measured with the 10-cm grid seems reasonable in view of other published work.

Figure 14 gives R_{uz} as a function of z/M, where M is the grid mesh dimension (10.16 cm in this case). When the area under the curve is computed, a value of the integral scale of ℓ_{uz} = 4.1 cm (1.6 in.) results. This is considered large enough to represent the upper range of interest in the study. The NACA 0015 airfoil being fabricated for this work has a chord of 40 cm and the boundary layer thicknesses will be far less than that.

It is interesting to find the corresponding microscale or dissipation scale. This is done by fitting a parabola to the data points on the left-hand side of Figure 14 in the range of $0 < z < 8$ mm, i.e., a parabola with its vertex at (1,0). This scale, which represents the typical dimension of the smaller eddies, in the z direction is found to be

$$\lambda_{uz} \approx 0.76 \text{ cm}$$

in this particular set of data.

Relative turbulence intensity in the 0.4-m test section when the 10-cm grid is installed has been found to be from 0.70 to 1.61 percent at 25.6 m/s, depending on grid location, and 0.77 to 1.77 percent at 50.1 m/s.

Dissipation Scale: A streamwise dissipation length scale is defined following Bradshaw, viz.,

$$L_{ux} = -(\overline{u^2})^{3/2}/[U_\infty(d\overline{u^2}/dx)]. \quad (7)$$

The longitudinal turbulence energy produced by grids typically decays according to a relation such as

$$(\overline{u^2}/U_\infty^2)^{-n} = C(x-x_0)/M, \quad (8)$$

where $\overline{u^2}$ = mean u^2 value,

C = a constant,

M = grid mesh size,

x = distance from grid and

x_0 = a constant.

There is frequent need for an effective starting length to be used in order to fit Eq. (8) to experimental data, thus x_0 is present to accommodate that need. When Eq. (8) is differentiated and combined with Eq. (7), it is found that

$$L_{ux}/M = nC^{-\frac{1}{2n}}[(x-x_0)/M]^{1-0.5/n}. \quad (9)$$

It is interesting to note that the scale will increase with x/M if n > 0.5 but decrease if n < 0.5.

Values of $\overline{u^2}/U_\infty^2$ have been measured with a hot-wire probe for various U_∞ and x, while the 10-cm grid was positioned at different distances upstream of the contraction section. This latter point is important; as the grid position changed, the intensity and scale at the entrance of the contraction changed. The findings reported in Ref. 11 show that the effect of the contraction depends on the turbulence characteristics of the entering flow. Thus, changing x by moving grids upstream of contractions while a probe is fixed in the test section may not produce the same variation of $\overline{u^2}$ with x as is produced when the grid is fixed and $\overline{u^2}$ is measured at

various longitudinal stations along the test section. Data to be taken during the remainder of this project will reveal more about this matter.

Figure 15 shows the variation of $\overline{u^2}/U_\infty^2$ as a function of x/M and Figure 16 shows the results when $(\overline{u^2}/U_\infty^2)^{-0.37}$ is plotted versus x/M. Table 2 gives the results when L_{ux} is computed by using Eq. (9) with these data.

TABLE 2. Typical Freestream Turbulence Characteristics with the 10-cm Grid*

U_∞ m/s	x/M	T'%	L_{ux} cm	L_{ux}/M
25.6	14.0	1.61	0.86	0.085
"	17.0	1.32	0.81	0.079
"	21.1	0.98	0.75	0.073
"	24.1	0.79	0.71	0.070
"	26.1	0.70	0.69	0.068
50.1	14.0	1.77	0.94	0.093
"	17.0	1.42	0.88	0.087
"	21.0	1.05	0.82	0.081
"	24.1	0.86	0.78	0.077
"	26.1	0.77	0.76	0.075

*These results obtained with hot-wire probe at fixed test section location and various grid locations upstream of contraction.

OTHER WORK

Computer programs for both laminar and turbulent boundary layers have been installed and checked out. These will be needed to support the research inasmuch as it is anticipated that the ratio of turbulence scale to boundary layer thickness will be a parameter useful in the analysis of the influence of scale on separation. The laminar flow code is of the finite-difference type, while the turbulent code is an integral method. Both have proved successful in comparisons with experimental data.

Fabrication of a NACA 0015 airfoil has begun. It will be the test

model on which boundary layer separation will be studied. To lessen flow blockage, only the upper surface of the airfoil will have the 0015 contour; the bottom surface will be flattened. However, a full leading-edge will be preserved. The material used is Plexiglas. Approximately 24 pressure orifices will be incorporated in the working surface. A chord of 0.406 m (16.0 in.) will result in a chord Reynolds number range up to 1.9×10^6. It had originally been planned to use a circular-arc airfoil for this work, but the change is being made so that the pressure distribution will be more conventional.

PROJECT STATUS AND PLANS

Owing to delays caused by equipment failures, conflict in demands for certain equipment which made it necessary to take earlier data manually, and a persistent problem with the hot-film probes, the amount of data collected by this time is somewhat less than expected. However, the last piece of equipment to fail, the TSI digital rms voltmeter, should be returned from the manufacturer in January, and the hot-film probes are being replaced by hot-wires wherever necessary. The automation of the measurement systems was partially completed late in this reporting period, and further improvement is planned in December and January. The delay caused by the most recent instrument failure is serious and it puts us at least one month behind schedule.

The taking of most of the data should proceed more rapidly, now that the techniques of the experimentation and measurement system refinements are in hand. Instrument failures could occur, but such delays should not be as time consuming as the developmental work already accomplished. Therefore, it is expected that the goals of this first year's work will be met, albeit somewhat later in the project period than originally planned.

A proposal to continue this research through a second year has been submitted to the NASA Langley Research Center Grants Office. This continuation would be for the purpose of analyzing the data in greater depth and making any additional measurements suggested following such analysis. A more thorough and useful research program would result.

REFERENCES

1. Bradshaw, P. An Introduction to Turbulence and its Measurement. Pergamon Press, Oxford, 1971.

2. Dryden, Hugh L., Schubauer, G. B., Mock, W. C., and Skramstad, H. K., "Measurements of Intensity and Scale of Wind Tunnel Turbulence and their Relation to the Critical Reynolds Number of Spheres". NACA Report No. 581, 1937.

3. Gorlin, S. M. and Slezinger, T. T. Wind Tunnels and Their Instrumentation. Translated by P. Boltiansky, Israel Program for Scientific Translations. Published as NASA TTF-346, Washington, DC 1966.

4. Schlichting, Hermann. Boundary Layer Theory, 4th edition, Translated by J. Kestin. McGraw-Hill, New York, 1960.

5. Hinze, J. O. Turbulence. McGraw-Hill, New York, 1959.

6. Townsend, A. A. Structure of Turbulent Shear Flow. University Press, Cambridge, 1956.

7. Batchelor, G. K. The Theory of Homogeneous Turbulence. University Press, Cambridge, 1956.

8. Hancock, P. E. and Bradshaw, P. "The Effect of Free-Stream Turbulence on Turbulent Boundary Layers". ASME Journal of Fluids Engineering, 105, 284, September, 1983.

9. Castro, T. P. "Effects of Free-Stream Turbulence on Low Reynolds Number Boundary Layers". ASME Journal of Fluids Engineering, 106, 298, September, 1984.

10. Bradshaw, P. "Effect of Free-Stream Turbulence on Turbulent Shear Layers". British A.R.C. 35648, 1974.

11. Tan-atichat, Jimmy, Nagib, Hassan M. and Drubka, Robert E. "Effect of Axisymmetric Contractions on Turbulence of Various Scales". NASA CR 165136, September 1980.

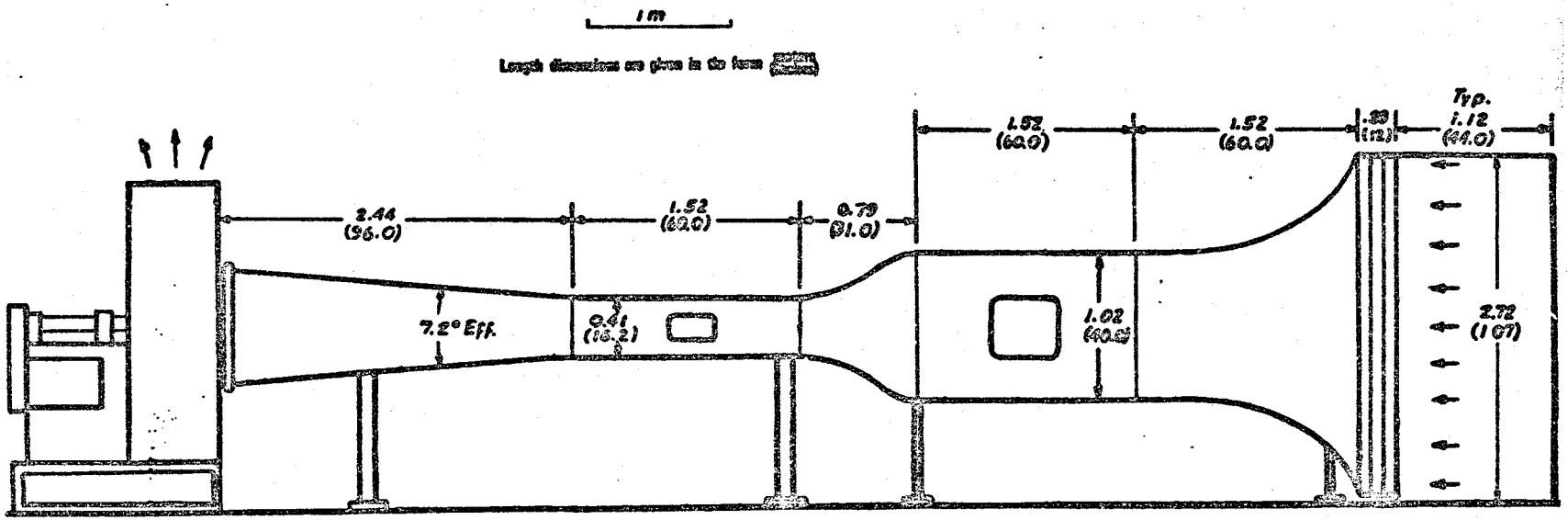

Figure 1. Vanderbilt Subsonic Wind Tunnel

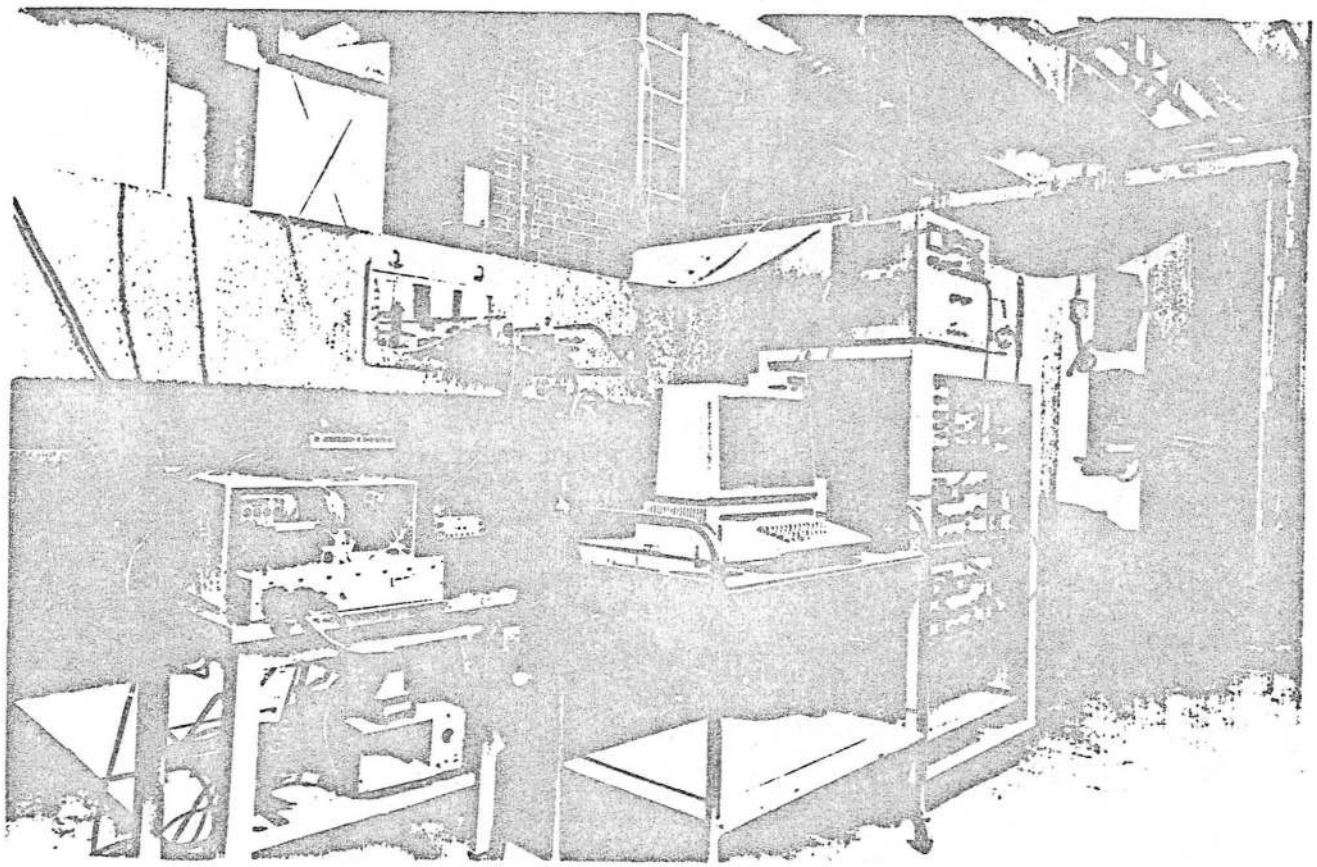

Figure 2. Photograph of 0.4-m Test Section and Instrumentation

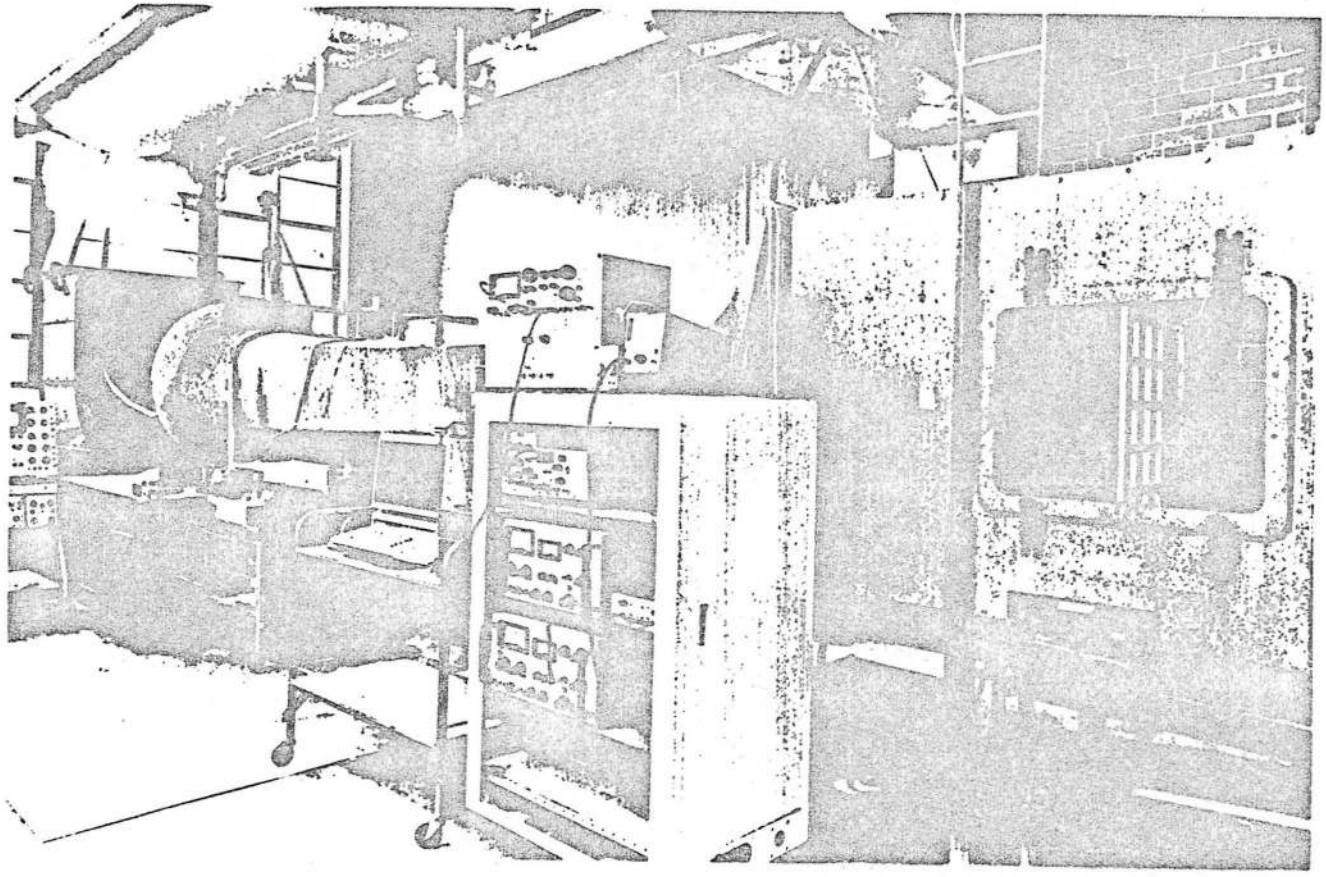

Figure 3. Photograph of 1-m Test Section Showing a Grid Installed

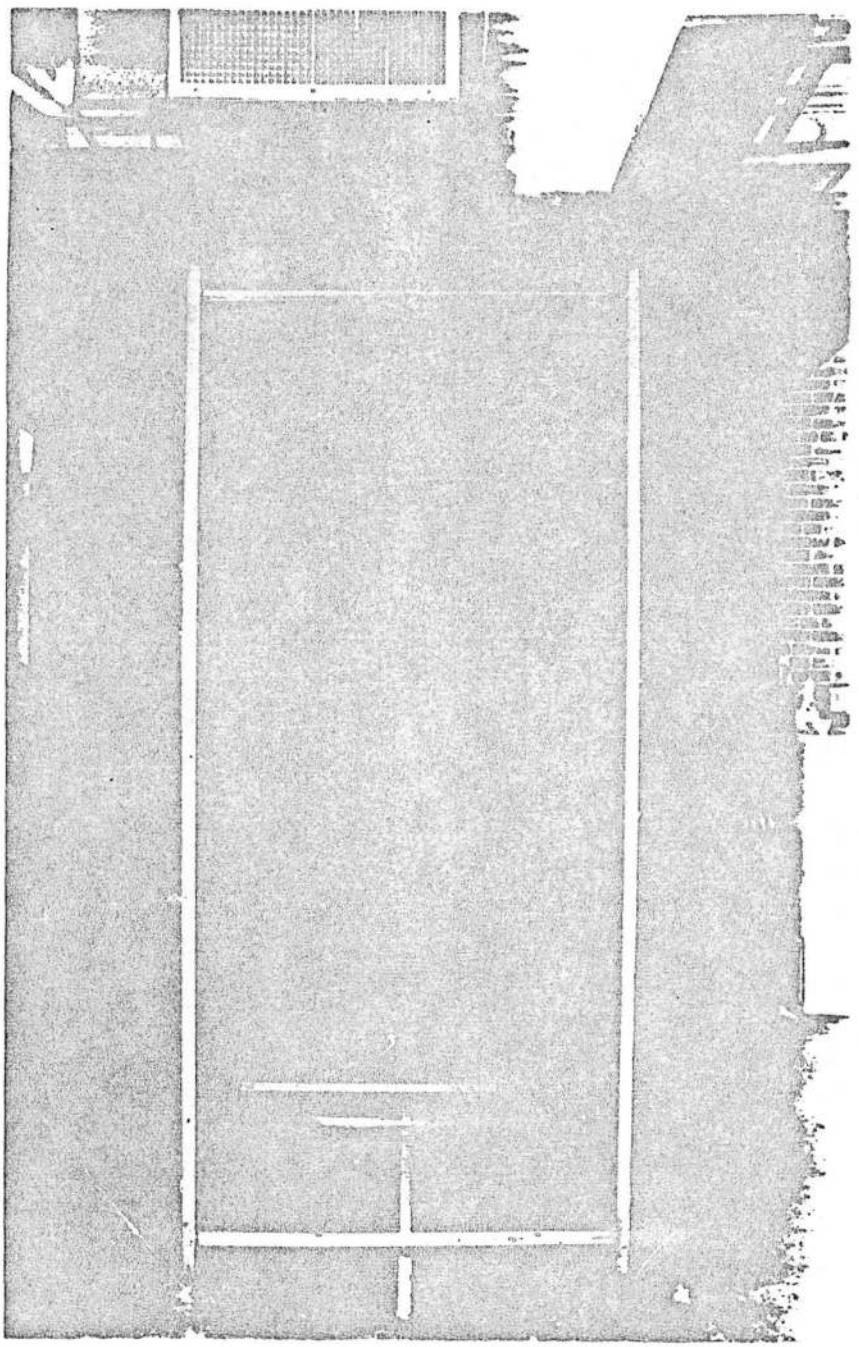

Figure 4. Entrance to Wind Tunnel Showing Shroud and Honeycomb

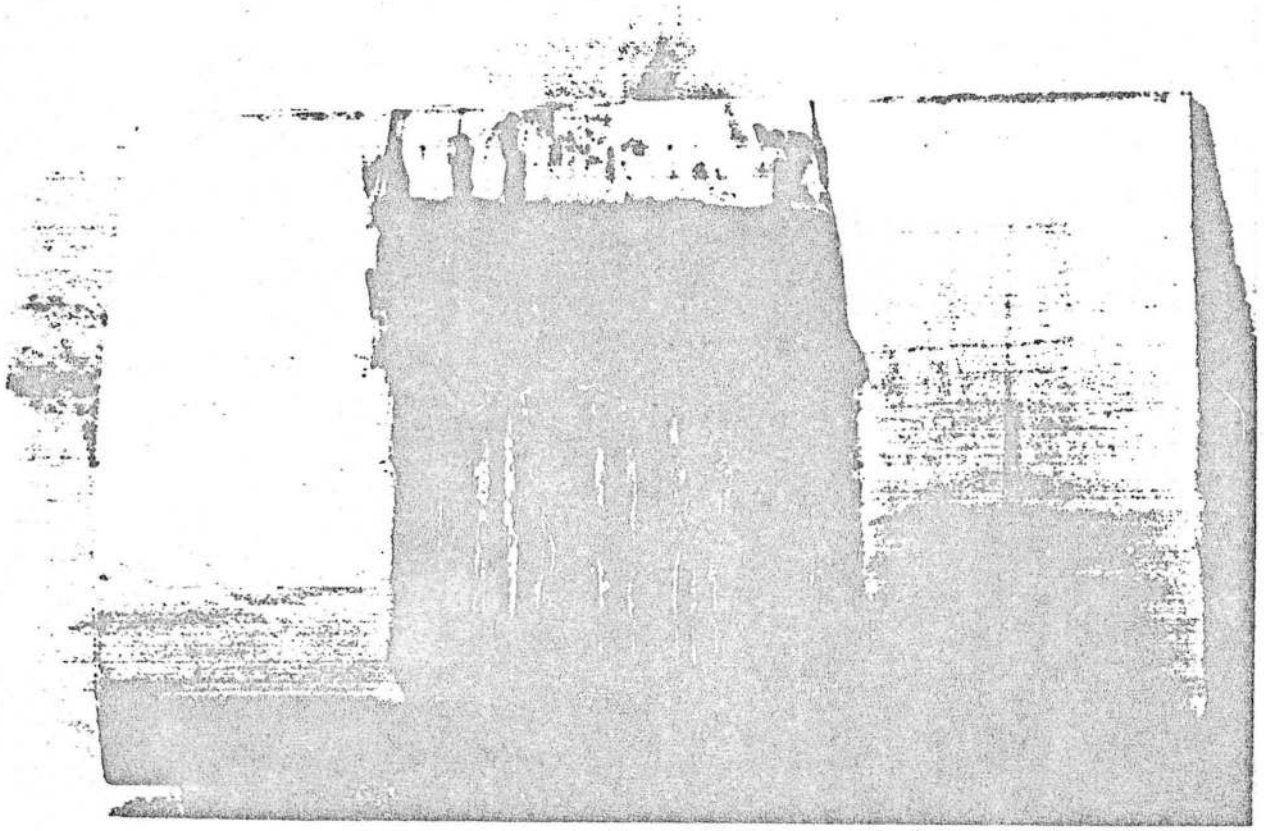

Figure 5.

Result of Using Liquid Film to Detect Separation Region on Airfoil

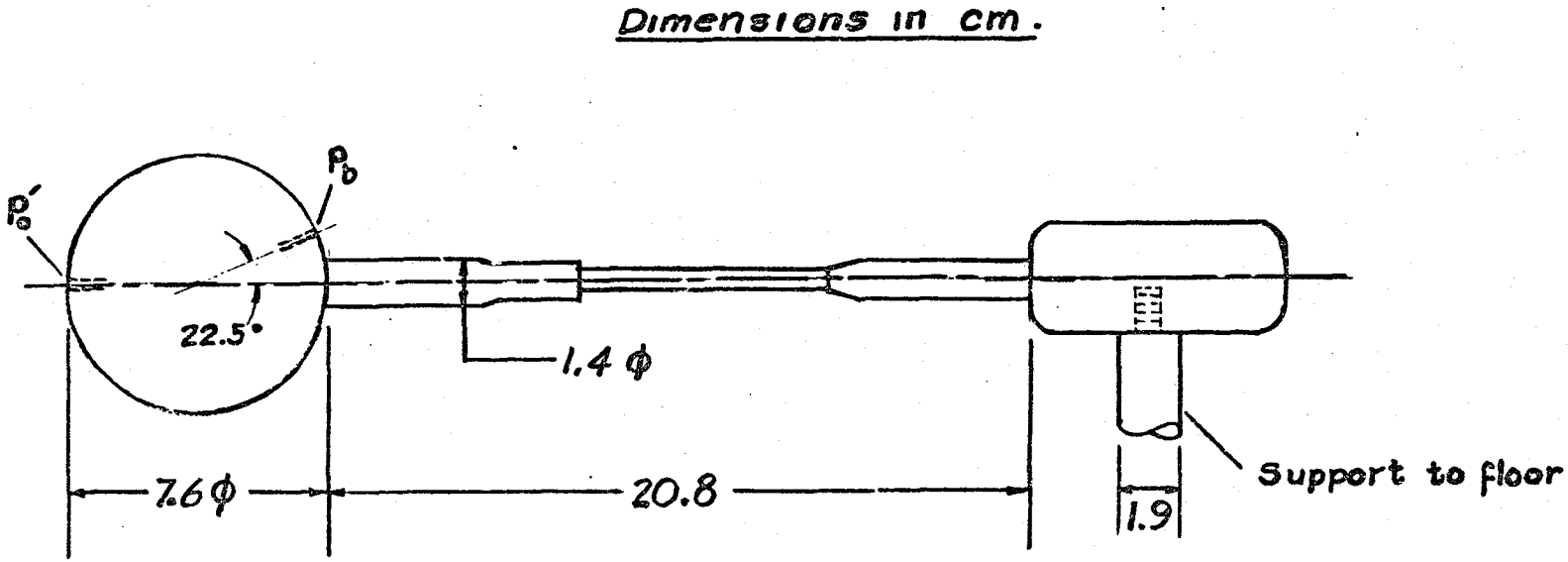

Figure 6. Sphere Used to Evaluate Wind Tunnel Turbulence

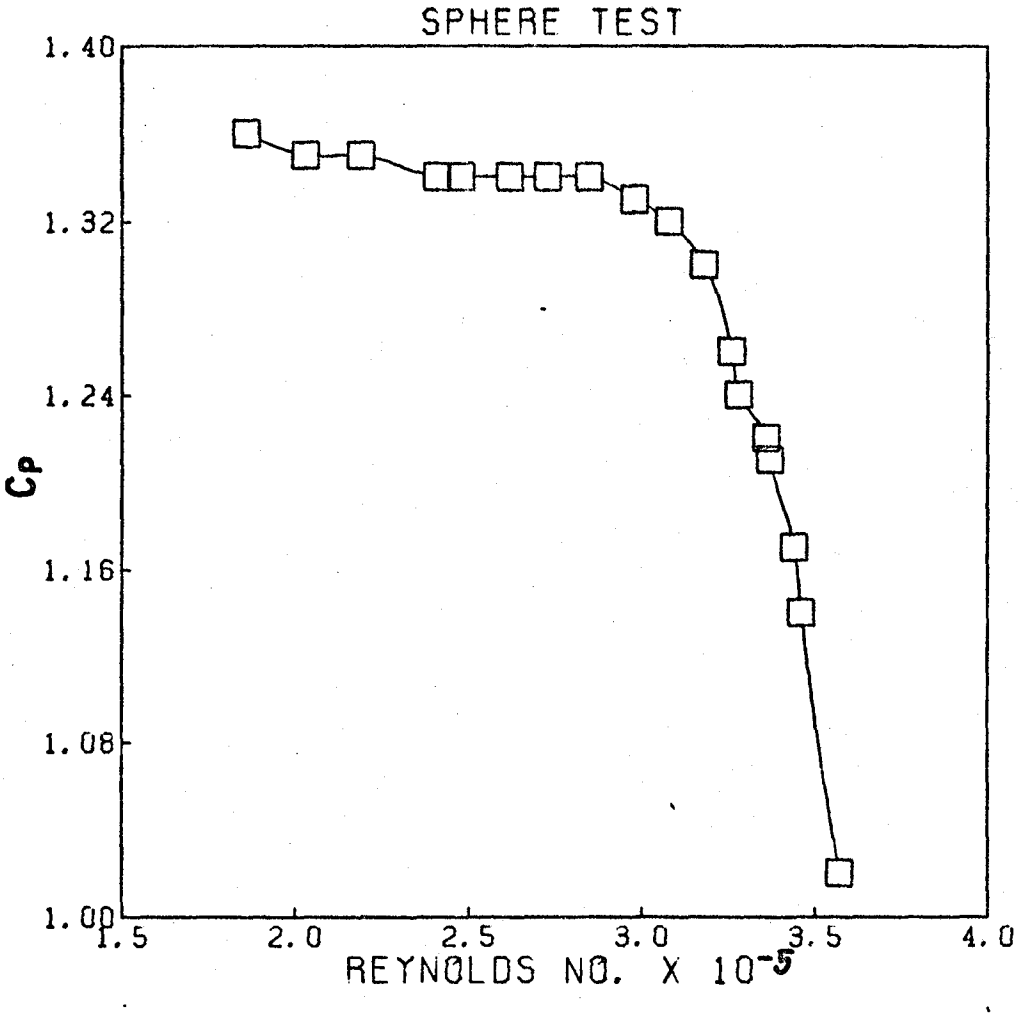

Figure 7.

Result of Sphere Critical Reynolds Number Experiment

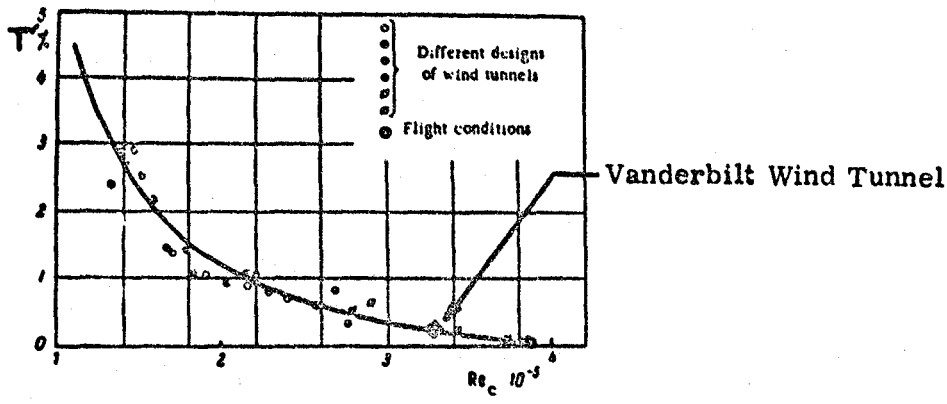

Figure 8. Correlation of Sphere Critical Reynolds Numbers and Relative Turbulence Intensities With Vanderbilt Turnel Data Point Shown

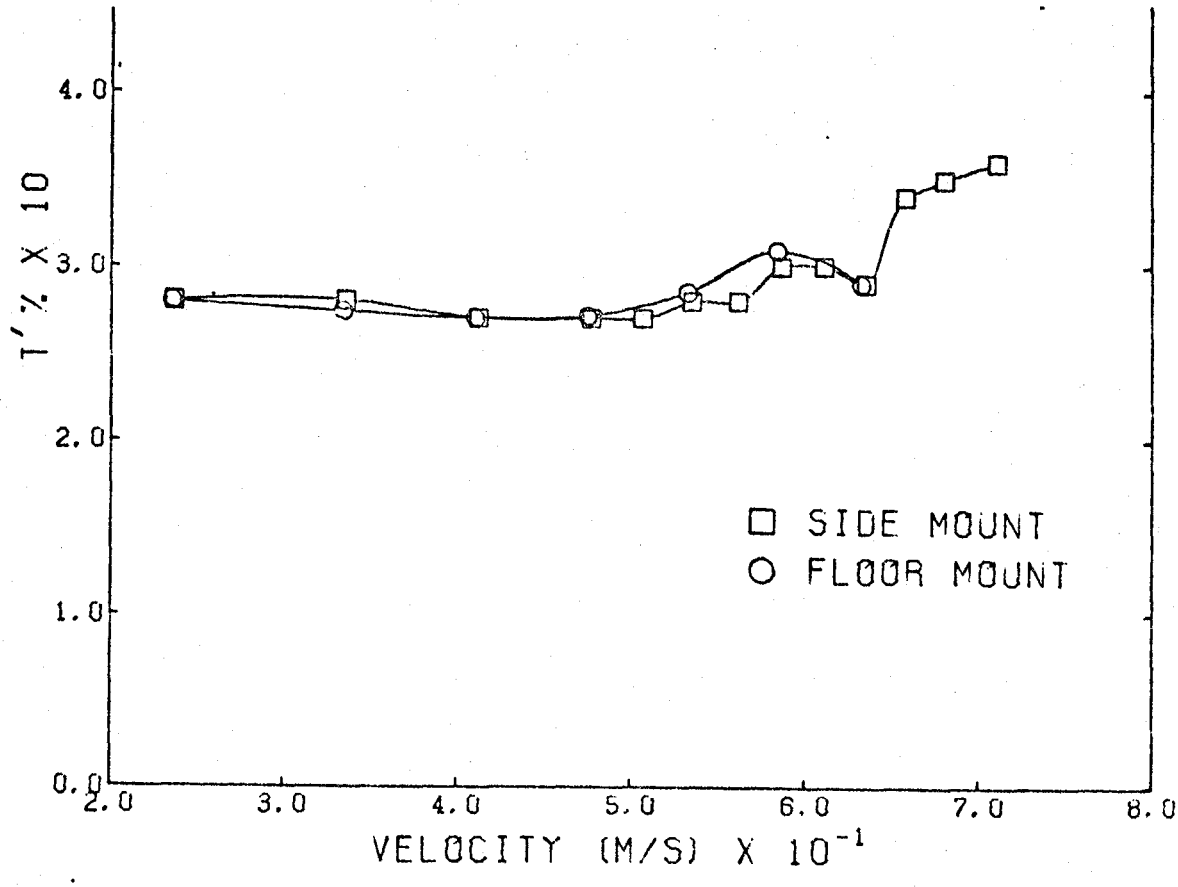

Figure 9. Relative Turbulence Intensity Measured by Hot-Wire Anemometer in the Vanderbilt Wind Tunnel

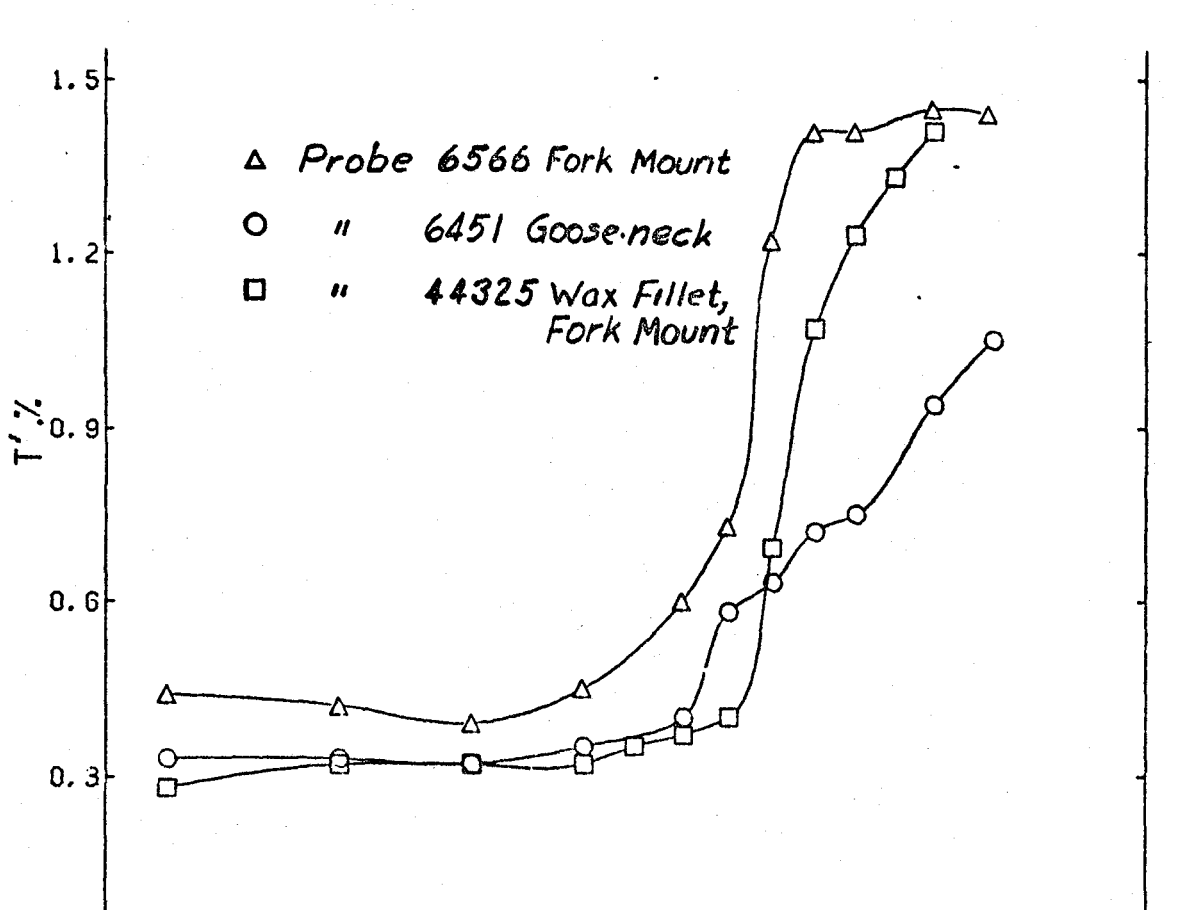

Figure 10. Relative Turbulence Intensity Measured by Hot-Film Probes

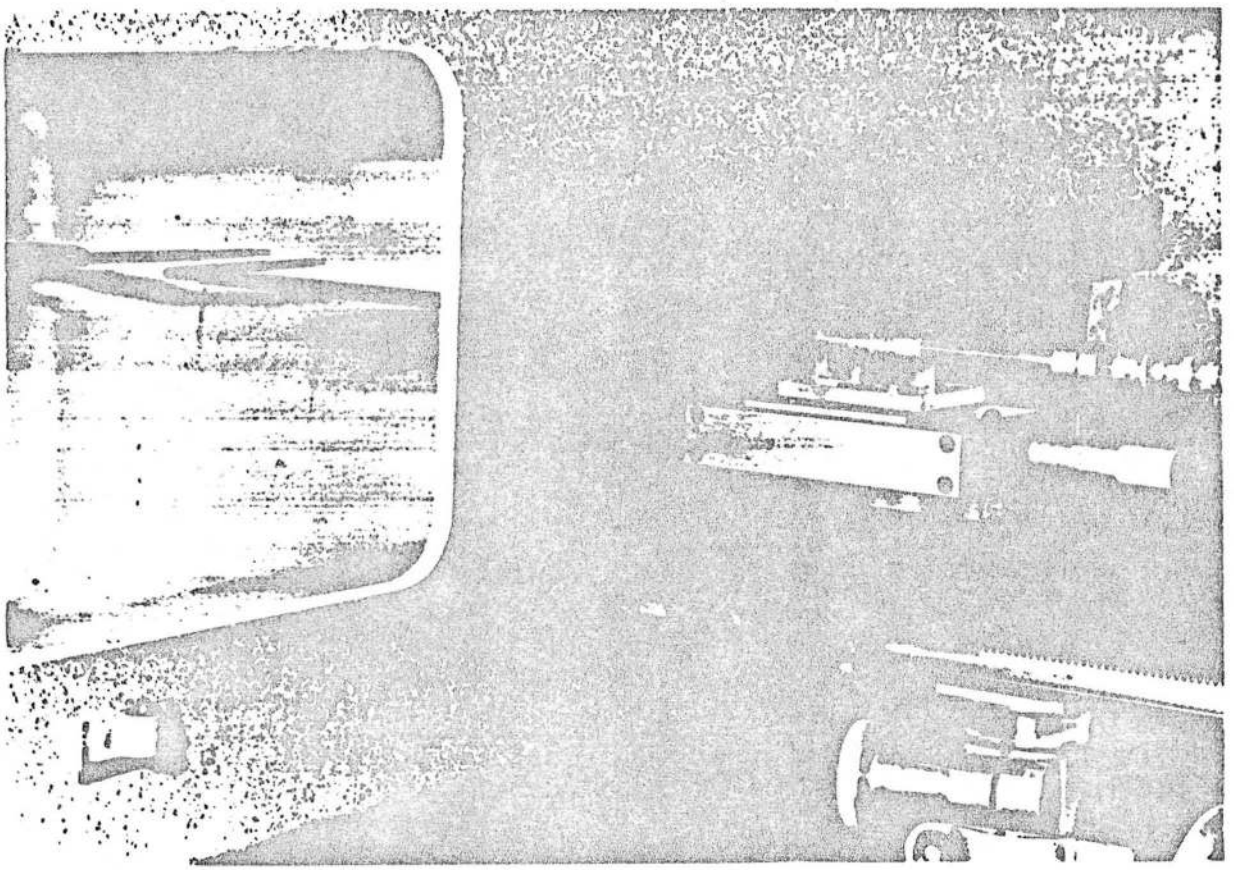

Figure 11. Hot-Wire/Hot-Film Probe Traversing System

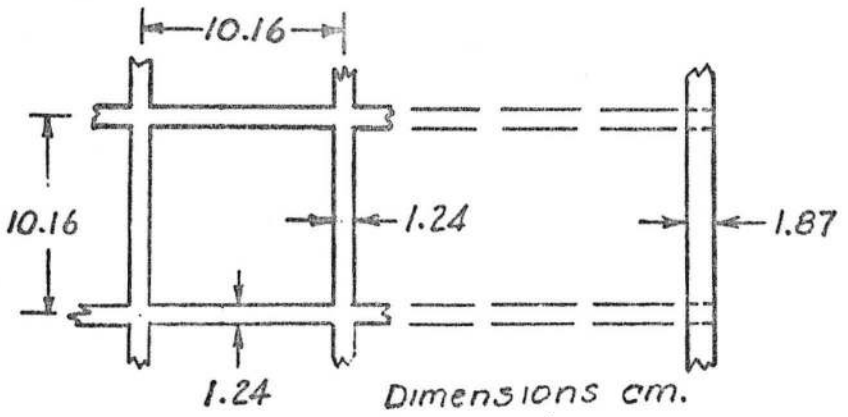

Figure 12. Dimensions of the 10-cm Turbulence Generating Grid

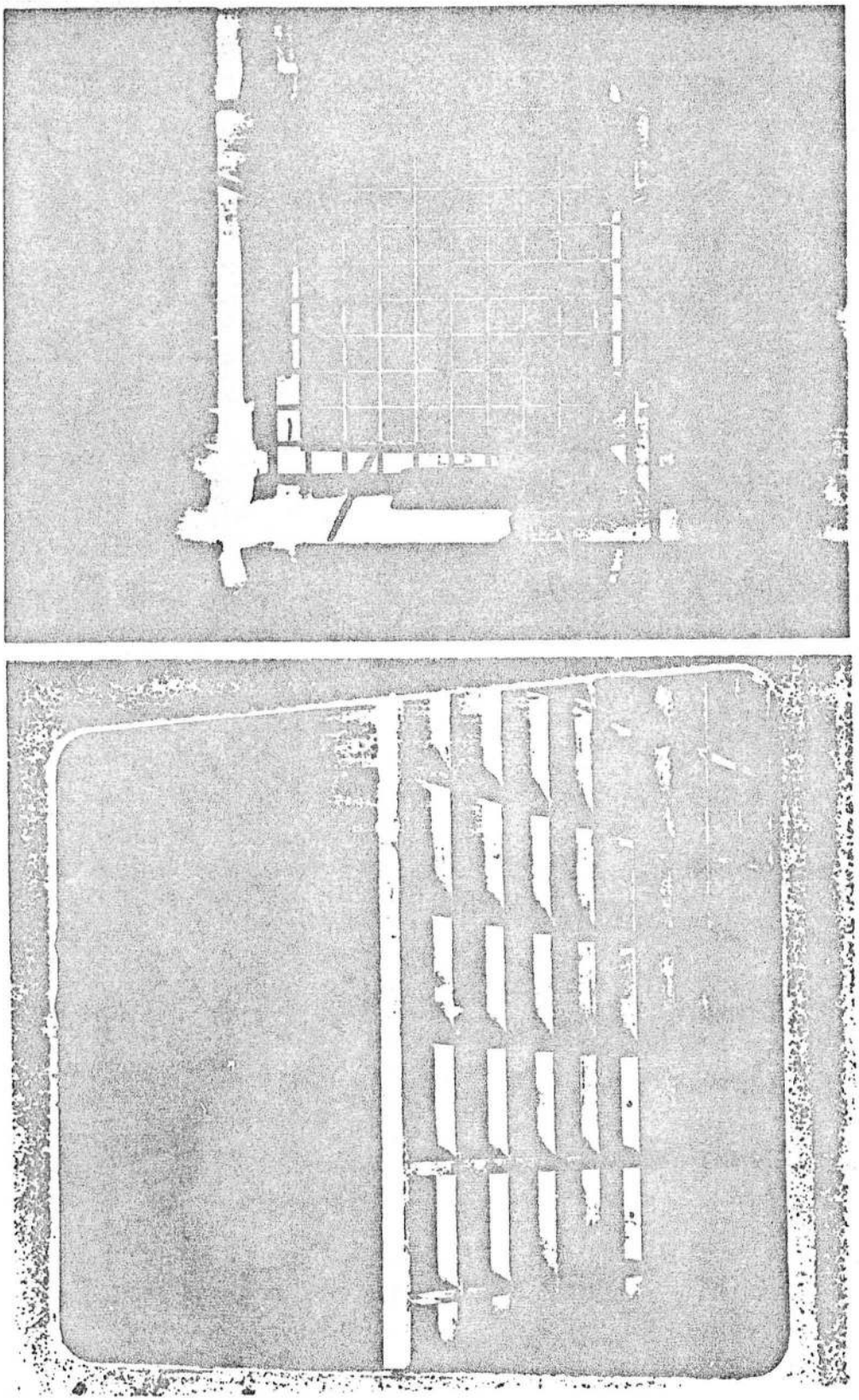

(a)

(b)

Figure 13. Photographs of the 10-cm Grid in the Tunnel

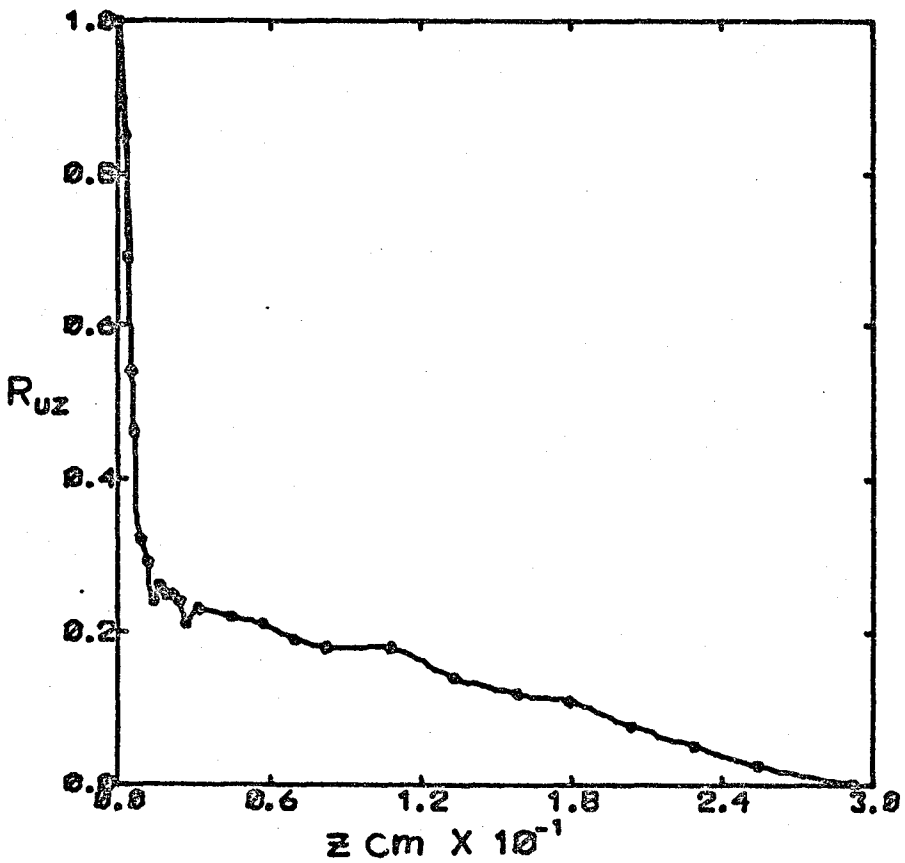

Figure 14. Lateral Correlation Coefficient as a Function of Probe Separation

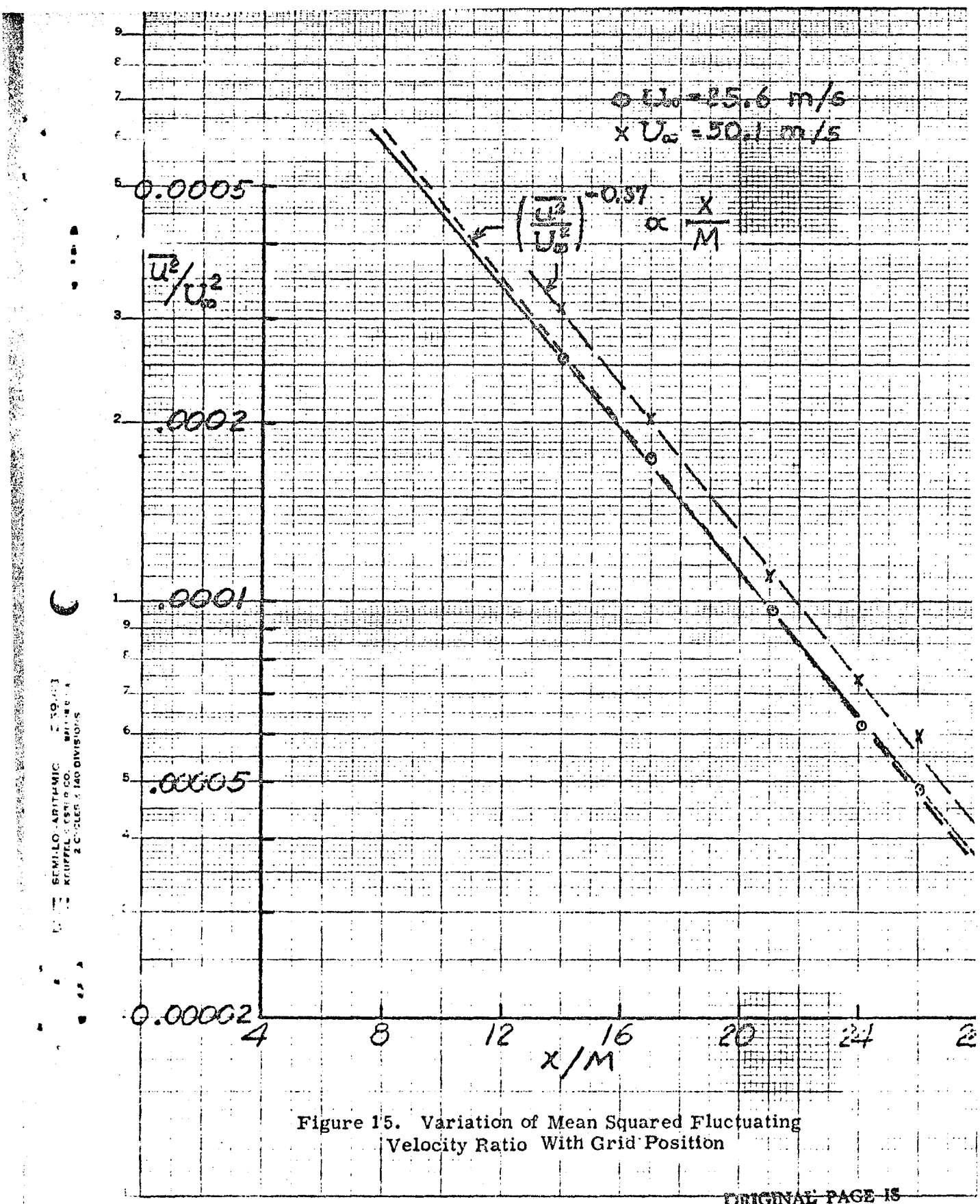

Figure 15. Variation of Mean Squared Fluctuating Velocity Ratio With Grid Position

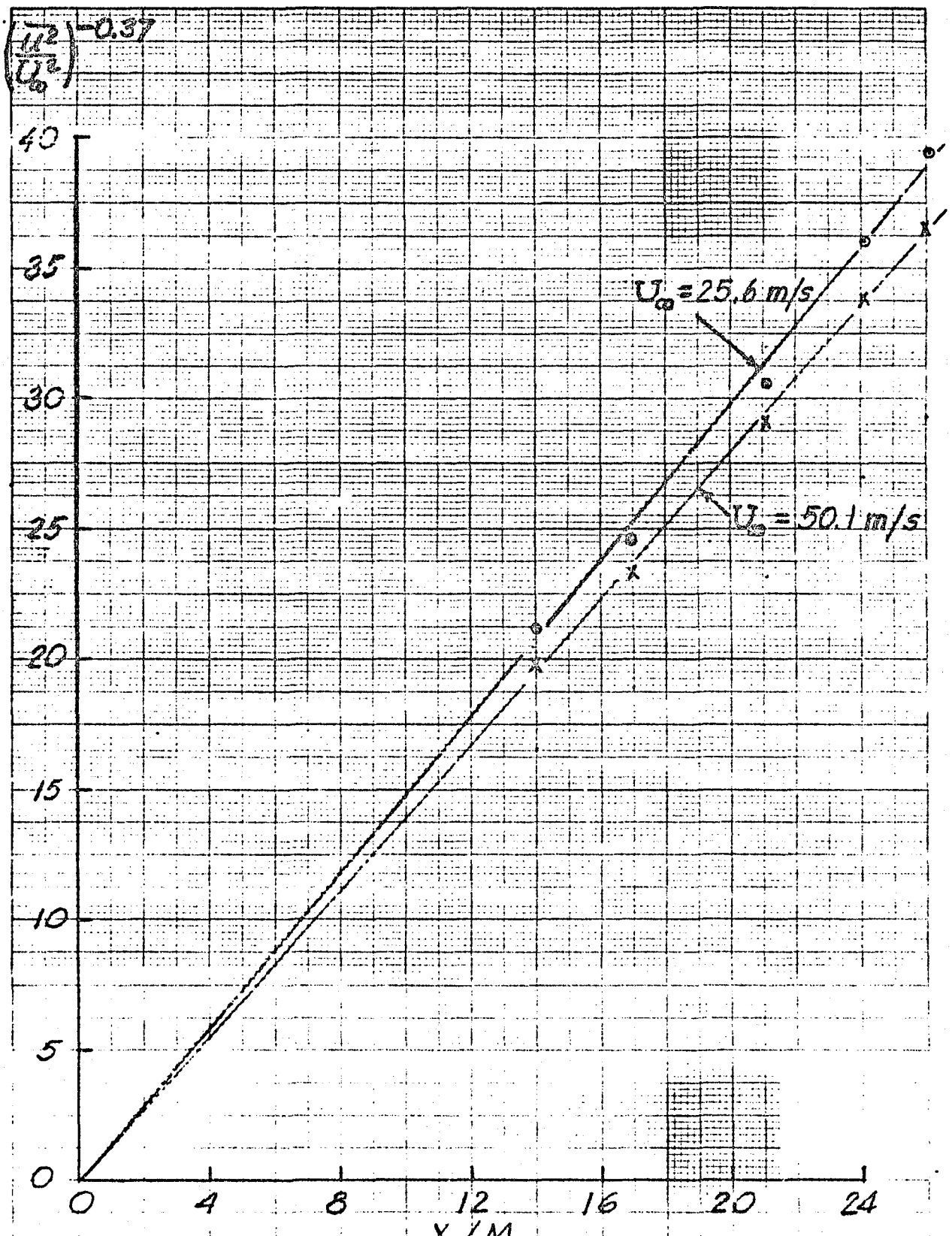

Figure 16. Linearization of $\overline{u^2}/U_\infty^2$ Data

END

DATE

FILMED

FEB 7 1985